Temperature Dependence of Raman Scattering and the Electro-Optic Properties of CuCl

I. P. Kaminow and E. H. Turner
Bell Telephone Laboratories, Holmdel, New Jersey 07733
(Received 15 September 1971)

The absolute Raman-scattering efficiencies, the clamped electro-optic coefficient r_{41}, and the dielectric constant κ of CuCl have been measured as functions of temperature. We confirm previous observations of four Raman lines: the longitudinal (LO), transverse (TO), and two second-order modes. The TO and a second-order mode have comparable strengths and are adjacent in frequency, giving the appearance of a double peak. The scattering efficiencies are nearly two orders of magnitude weaker in CuCl than the LO and TO modes in GaAs. Proper mode assignments and relative scattering efficiencies are discussed. Both κ and r_{41}, measured at 0.633 and 3.39 μm, decrease appreciably as the temperature is reduced from 300 to 90 °K. It is shown that the magnitude and sign of the nonlinear optical coefficient d_{14}^0 as well as the ratio C of the lattice and electronic contributions to r_{41} can be determined from these temperature-dependent r_{41} and κ measurements alone. Attempts to determine d_{14}^0, r_{41}, and C from the Raman measurements alone, as had been done in GaAs, are complicated by the double-peaked TO mode, but such a correlation is possible. The parameters of a simple bond-charge model (including effective charge, spring constant, and Raman polarizability) for CuCl and GaAs are calculated and compared. The signs of the effective charges on Cu and Ga are found to be opposite. The results are discussed in terms of the relative ionicities (low for GaAs and high for CuCl) of the two compounds.

I. INTRODUCTION

Cuprous chloride is a member of the wide class of binary semiconductors having the cubic zinc-blende structure. Many of these crystals have interesting applications in electro-optic and nonlinear-optic devices. Because of their structural similarity and simplicity, the nonlinear optical properties of the zinc-blende materials have been the subject of recent theoretical studies. An important parameter employed to characterize members of the class is the ionicity f_i, or its complement the covalency $1-f_i$, of the bonding. These rather nebulous qualities have been put on a quantitative basis for a variety of crystals by Pauling[1] and by Phillips and VanVechten.[2] On such a scale, $f_i = 0$ (covalent) for Si, $f_i = 0.31$ (moderately covalent) for GaAs, and $f_i = 0.75$ (moderately ionic) for CuCl. The ionicity of CuCl is close to the maximum found for zinc-blende materials; more ionic binary compounds crystallize in the rock-salt structure. Its borderline position and high ionicity make CuCl an interesting crystal to study and compare with the more covalent zinc-blende materials like GaAs. We have measured the Raman spectrum and electro-optic coefficients of CuCl and find that its behavior is anomalous in several respects when compared with GaAs.

The zinc-blende structure contains two atoms in the primitive cell so that there is only one triply degenerate fundamental optic mode, which is both Raman and infrared active. This mode is split into a transverse (TO) and a longitudinal (LO) mode by the macroscopic electric field. The Raman spectrum[3] of GaAs consists of strong TO and LO lines and very weak second-order bands. Early Raman measurements[4] on CuCl indicated only a TO and LO mode but later infrared[5] and Raman[6] experiments showed four peaks. The TO and LO modes are much weaker than in GaAs, and two second-order bands have strengths comparable to the fundamentals. The TO mode appears to have a curious double peak: One peak is the fundamental and the other a second-order mode. It has not been possible to identify one peak or the other unequivocally with the fundamental TO mode. For this reason, calculation of dielectric constants, effective charges, and nonlinear coefficients based on TO- and LO-mode observations are ambiguous. Previous assignments of the TO mode[4-6] are contradicted by our observations. Temperature-dependent Raman measurements of *absolute* scattering efficiency of these four peaks are discussed in Sec. II.

Measurements of the constant-strain electro-optic coefficient r_{41} at 0.633 and 3.39 μm were made as a function of temperature. These results together with measurements of the temperature dependence of constant-strain dielectric constant κ are reported in Sec. III. Both r_{41} and κ change appreciably in the temperature range investigated and since the behavior of each of these quantities is related to the same Raman- and infrared-active mode, we use this change to separate the purely electronic and lattice-dependent components of r_{41}. It is then possible for the first time to make reliable predictions about both magnitude and sign of the purely electronic nonlinear optic coefficient d_{14}^0 from electro-optic behavior alone.

The spontaneous Raman-scattering efficiency and

the electro-optic and nonlinear-optic coefficients r_{41} and d_{14}^0 are closely related. These optical coefficients can be accurately determined from absolute Raman measurements for GaAs.[7] Attempts to apply the same formalism to CuCl are complicated by the presence of the relatively strong second-order lines, which cannot be ignored. Still, with suitable interpretation of the Raman spectrum, in Sec. IV we calculate values for r_{41} and d_{14}^0 in CuCl that agree with directly measured values within experimental uncertainty.

Finally, in Sec. V, we compare observed and calculated properties (such as effective charges, spring constant, and Raman polarizability) of CuCl and GaAs on the basis of a simple bond model. Experiment indicates that the ionic charges on Cu and Ga have opposite sign. The general trends agree with our intuitive notions of ionic-covalent bonding.

II. RAMAN-SCATTERING MEASUREMENTS

A. Experiment and Results

1. *Crystals*

Flux and melt-grown[8] crystals with dimensions greater than 1 cm were generously provided by Inoguchi of the Sharp Corp., Japan, and gel-diffusion-grown[9] crystals with a perfect tetrahedral habit, 4 mm on an edge, were generously provided by Armington of the Air Force Cambridge Research Center. Both types of crystals give similar results. However, the gel-diffusion crystals, which are grown at room temperature, are virtually free of strain birefringence. Since strain birefringence introduces spurious lines in polarized Raman spectra, the smaller crystals were used in spite of the added difficulties in handling and signal strength.

The tetrahedral edges of the crystal habit lie along ⟨110⟩ axes. Two {110} faces, approximately 1 mm^2, were polished normal to and at opposite ends of an edge. Then a 1×4 mm {001} face was polished parallel to the edge and normal to the end faces. With this geometry the incident beam propagates in the [110] or X' direction and the light scattered at 90° is observed along the [001] or Z direction.

2. *Absolute Scattering Efficiency*

The Raman measurements reported here were made at 0.633 μm in order to avoid the dispersion effects of strong CuCl exciton bands at 0.39 μm.

The absolute scattering efficiency $S_B/L\,d\Omega$ of the totally symmetric 992-cm^{-1} line in benzene has been determined at 0.488 μm by Skinner and Nilsen.[10] This line is a convenient reference standard for measuring the efficiency of other lines. Applying the λ^4 law to their 0.488-μm measurement, we find $S_B/L\,d\Omega = 1.0\times10^{-7}$ cm^{-1} sr^{-1} at 0.633 μm. We have confirmed this extrapolation by direct measurement of benzene at 0.633 μm using a standard lamp for calibration.

The efficiency of an unknown line, designated by subscript i, as well as its natural linewidth $2\Gamma_i$, can be obtained by comparison of areas A_i and A_B under the spectral distribution curves of the unknown and benzene for identical experimental conditions.[11] Thus

$$\frac{S_i}{L\,d\Omega} = G\left(\frac{S_B}{L\,d\Omega}\right)\left(\frac{A_i}{A_B}\right)\left(\frac{P_B}{P_i}\right)\left(\frac{L_B}{L_i}\right)\left(\frac{n_i}{n_B}\right)^2\left(\frac{T_B}{T_i}\right)\left(\frac{\eta_B}{\eta_i}\right), \quad (1)$$

where G is a geometrical factor to be discussed later, (P_B/P_i) is the ratio of incident powers, (L_B/L_i) is the ratio of scattering path lengths, $(n_i/n_B)^2$ is the ratio of refractive indices squared which is inversely proportional to the ratio of collection solid angles $d\Omega$, (T_B/T_i) is the ratio of powers transmitted through the two samples including reflection, scattering, and absorption losses, and (η_B/η_i) is the ratio of detection sensitivities at the appropriate Stokes frequencies as determined by a standard lamp.

The linewidth $2\Gamma_i$ can be obtained from Raman spectral curves using the chart in Ref. 11 to eliminate the spectrometer function.

A Spex double monochromator with cooled RCA C70042K (extended red) photomultiplier and Keithley dc ammeter were used to observe spectra. It is important to keep the photomultiplier temperature constant from run to run in order to maintain constant sensitivity. Widths of 300, 350, and 300 μm for input, middle, and exit slits, respectively, give a resolution of 8 cm^{-1} and reasonable signal-to-noise ratio. A Polaroid circular polarizer at the input slit was used to select the scattered polarization and scramble the polarization incident on the gratings. The polarized output of a He-Ne laser was focused into the sample by a 20-cm focal-length lens and the scattering path imaged onto the slit by a 7.5-cm lens stopped down to match the f number of the monochromator. The incident He-Ne laser beam was filtered to eliminate the weakly oscillating 0.640-μm radiation which would obscure an important portion of the Raman spectrum. The sample is cooled by an Air Products Joule-Thomson nitrogen refrigerator with windows for input, transmitted, and scattered beams. The incident power P is measured before the input lens and the relative transmission is measured beyond the sample, outside the refrigerator. The incident power is limited to about 20 mW in order to avoid damaging the sample.

The beam passing through the CuCl crystal is not appreciably depolarized by strains. The refractive index[12] of CuCl at 0.633 μm, $n = 1.96$, gives a reflection of 11% per surface. However,

the total transmission through the crystal along a path $L = 4.2$ mm is only 20%, independent of temperature, due to bulk absorption and scattering as well as poor surface quality.

3. *Spectra*

The triangular Stokes spectrum of the benzene sample is shown in Fig. 1, where photomultiplier current is plotted against Stokes shift. The dark current I_D obtained by closing the input slit is also indicated. The area under the curve above the background, normalized to length and incident power, is

$$(A_B/L_B P_B) = 332\times 10^{-9}\ \text{Å cm}^{-1}/\text{cm W}. \qquad (2)$$

The base width of the triangular function is $2b = 16.5$ cm^{-1}. The natural linewidth of benzene[10] is 2.3 cm^{-1}. We have also made use of this 992-cm^{-1} line to calibrate the Stokes-shift frequency scale in all the spectra presented below.

Four scattering geometries are possible with the tetrahedral crystal having incident beam along X' and scattered beam along Z. The selection rules for the fundamental optical phonon allow both LO and TO for $X'(Y'Y')Z$ and $X'(ZX')Z$, allow only TO for $X'(ZY')Z$, and allow no fundamental Raman scattering for $X'(X'Y')Z$, where the polarization directions for incident and scattered light, respectively, are given inside the parentheses. In the $X'(ZY')Z$ geometry, the induced phonon travels in the $X'Z$ plane at 45° to the Z axis and is polarized along Y', which is transverse to the direction of propagation. In the $X'(Y'Y')Z$ geometry, the induced phonon travels in the same direction but is polarized along Z and has equal TO and LO components. For the same incident power, the observed strength of the TO mode in the latter case will be half that in the former case and the LO-mode strength will be half what it would be if the LO mode alone could be excited directly. Thus, in order to find the intrinsic scattering efficiencies for these modes,[7] the geometrical factor in (1) is 2 for $X'(Y'Y')Z$ and $X'(ZX')Z$ and unity for $X'(ZY')Z$.

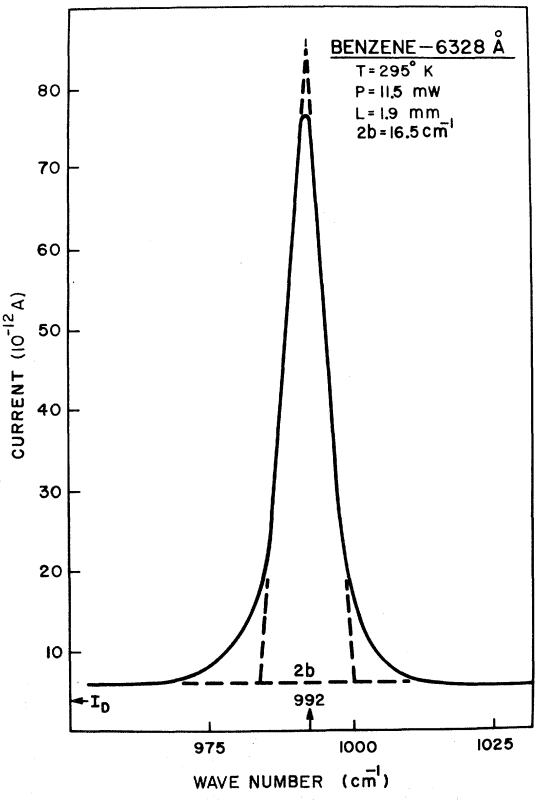

FIG. 1. Raman spectrum of 992-cm^{-1} benzene line. Photomultiplier current vs Stokes shift.

Figures 2(a)–2(e) show $X'(Y'Y')Z$ spectra at five temperatures ranging between 105 and 295 °K. The noise-limited vertical resolution and slit-limited horizontal resolution are indicated by the cross-hatched boxes in the figures. These spectra are characterized by four peaks which we label $\bar{\alpha}$, $\bar{\beta}$, $\bar{\gamma}$ and $\bar{\delta}$ beginning with the lowest frequency. Similar spectra are observed with the $X'(ZX')Z$ geometry. In the $X'(ZY')Z$ geometry, only the $\bar{\delta}$ peak is absent. Thus, $\bar{\delta}$ is the LO mode. In the $X'(Y'X')Z$ geometry all four peaks are absent, indicating that $\bar{\alpha}$, $\bar{\beta}$, and $\bar{\gamma}$ obey the selection rule for TO and that strain does not introduce spurious lines. These observations are consistent with those reported by Krauzman.[6]

The three high-frequency lines are well resolved only at low temperature. However, one can do a reasonable job of separating the spectra into four symmetric lines that conserve the total area under the curve for all spectra. The ambiguity in the separation increases with the temperature T. The peak frequencies $\nu = \omega/2\pi c$, linewidths 2Γ, and scattering efficiencies $S/L\,d\Omega$ (using $G = 2$) for these lines are tabulated in Table I. The absolute scattering efficiencies are difficult to measure accurately because the modes are weak, the background level is relatively high, and the sample transparency is poor. We estimate that the absolute values may be in error by as much as a factor of 2. However, relative values should be less uncertain. The table also contains data for the geometric mean of the frequencies of the $\bar{\beta}$ and $\bar{\gamma}$ lines and the scattering efficiencies for the sum of $\bar{\beta}$ and $\bar{\gamma}$ for later use; these quantities are designated by $\overline{\beta\gamma}$. In addition the table contains the Bose factors $(\bar{n}_i + 1)$, with $\bar{n}_i = (e^{\hbar\omega_i/kT} - 1)^{-1}$ and ω_i the appropriate angular frequency.

The Stokes scattering efficiency for a fundamental phonon is proportional to $(\bar{n}_i + 1)$. For a two-phonon sum mode the efficiency is proportional to $(\bar{n}_i + 1)(\bar{n}_j + 1)$ and for a difference mode the effi-

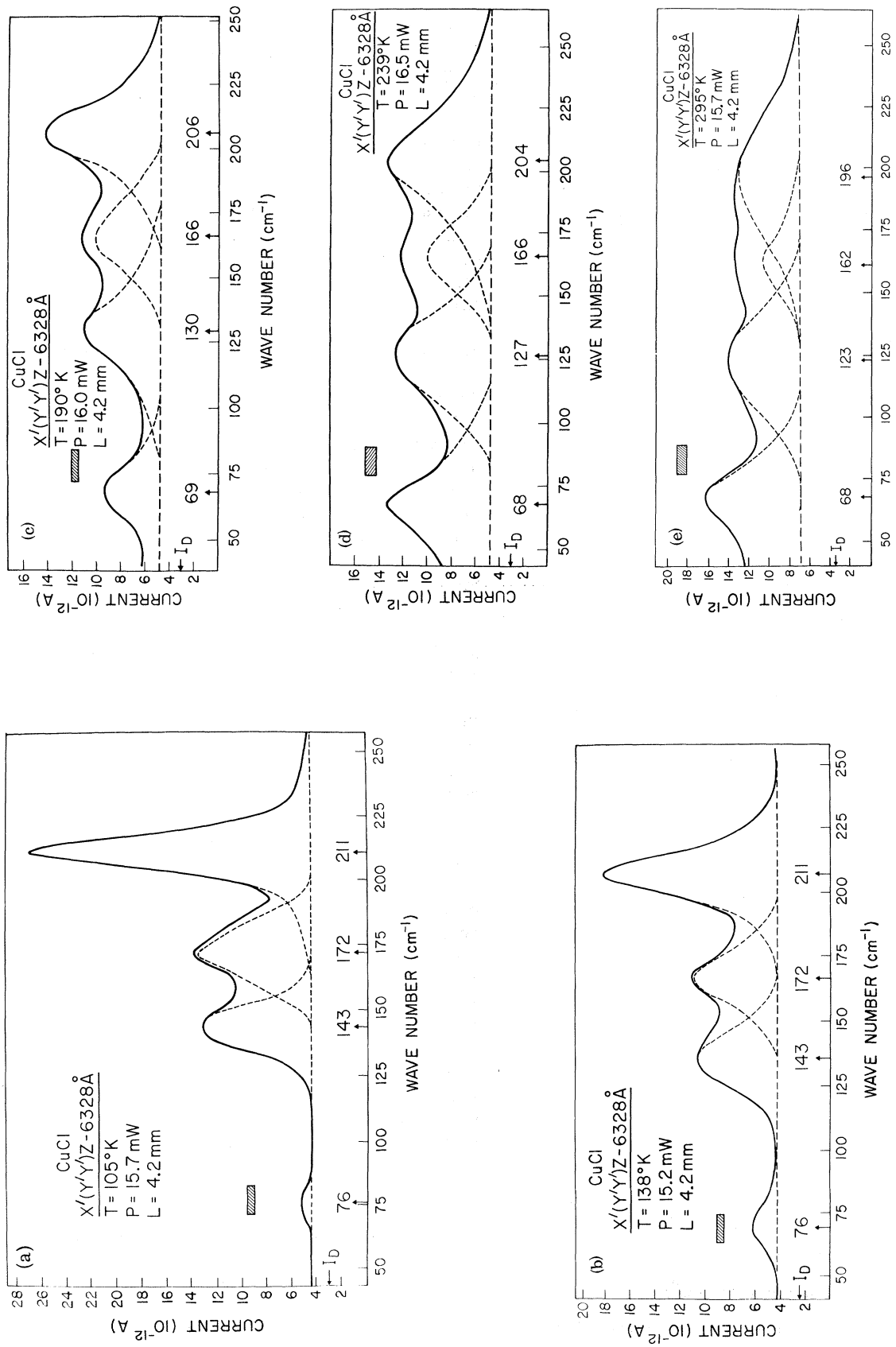

FIG. 2. Raman spectra of CuCl. Photomultiplier current vs Stokes shift. Cross-hatched box indicates vertical (noise) and horizontal (slit) resolution. Same conditions as Fig. 1: (a) 105 °K, (b) 138 °K, (c) 190 °K, (d) 239 °K, (e) 295 °K.

ciency is proportional to $\bar{n}_i(\bar{n}_j+1)$, where $\bar{n}_i$ and $\bar{n}_j$ refer to the two participating phonons. Each of these three factors increases with increasing T but the rate of increase in the difference-mode factor is fastest because $\bar{n}_i \to 0$ as $T \to 0$. From Table I, it is clear that the temperature dependence of scattering efficiency for the $\bar{\alpha}$ mode behaves like that for a two-phonon difference mode. Thus, we identify $\bar{\alpha}$ as a two-phonon difference mode. The temperature dependence of the $\bar{\delta}$-mode strength corresponds to $(\bar{n}_\delta+1)$ within experimental uncertainty as it should for a fundamental LO mode.

The temperature behavior of the $\bar{\beta}$- and $\bar{\gamma}$-mode strengths is less clear. While the $\bar{\beta}$-mode strength follows $(\bar{n}_\beta+1)$ reasonably well, the scattering efficiency of the $\bar{\gamma}$ mode *decreases* as T increases, and does not fit either a one- or two-phonon factor.

B. Discussion

The CuCl spectrum exhibits a number of unusual features when compared with the well-behaved spectrum of GaAs.[7] The room-temperature scattering efficiencies of GaAs LO and TO modes at 1.06 μm are 2.3×10^{-6} and 1.5×10^{-6} cm^{-1}, respectively, and, assuming the λ^4 law, would be 1.8×10^{-5} and 1.2×10^{-5} cm^{-1} at 0.633 μm. These values are nearly two orders of magnitude greater than the CuCl efficiencies listed in Table I. The two-phonon lines in GaAs are about an order of magnitude weaker than their fundamentals[3] and there is no confusion in identifying the LO and TO; whereas the one- and two-phonon lines have comparable strength in CuCl. The room-temperature CuCl linewidths are more than an order of magnitude greater than the GaAs linewidths which are $2\Gamma_L = 1.6$ cm^{-1} and $2\Gamma_T = 1.7$ cm^{-1}. These distinctions can be traced to differences in binding forces, anharmonicity and ionicity.

The resonant TO frequency of a binary lattice is given by an effective mass $\bar{m}$ and force constant K: $K=\bar{m}\omega_0^2$. Taking the frequencies and effective masses of GaAs and CuCl as 270 and 123 cm^{-1}, and 36 and 23, respectively, we find $K(\text{GaAs}) = 7.3K(\text{CuCl})$: The CuCl spring is much softer than the GaAs spring. The mean-square lattice displacement is given by $K\overline{X^2} \sim kT$ and at room temperature $(\overline{X^2})^{1/2}(\text{CuCl}) = 2.7\,(\overline{X^2})^{1/2}(\text{GaAs})$. The temperature of CuCl must be reduced to 40 °K in order to reduce fluctuations in bond length to the level found in GaAs at room temperature. Thus, with the softer lattice, one expects anharmonic effects and line broadening in particular to be more pronounced in CuCl.

The ionicity of CuCl is the largest of any zinc-blende material and is just below the critical ionicity above which the rock-salt structure is preferred.[2] In an ionic substance the optically polarizable charge is located on an ion core and moves with it, while in a covalent substance the polarizable charge is localized near the center of the bond. Since the charge is associated with the bond in the latter case, one expects fluctuations in bond length to produce greater perturbations of optical polarizability, yielding greater Raman-scattering efficiency in covalent than in ionic crystals (see Sec. V).

The $\overline{\beta\gamma}$ double peak is the most anomalous feature of the CuCl spectrum. It is present in the several crystals from two sources we have examined, and has also been observed by Krauzman.[6] X-ray powder patterns show the structure of our crystals to be fcc with $a = 5.41$ Å as expected for the zinc-blende structure.[13] Isotope effects are too small to account for the observed splitting.

A double peak at 149 and 178 cm^{-1} at 100 °K is also observed in infrared-absorption spectra.[5] The higher-frequency ($\bar{\gamma}$) component is the stronger at 300 °K but the two components have comparable strengths at 100 °K. The behavior of relative infrared strengths contrasts with that of the Raman strengths for which the lower-frequency ($\bar{\beta}$) component is the stronger at 300 °K, while $\bar{\beta}$ and $\bar{\gamma}$ again have comparable strengths at 100 °K. At 4 °K, a low-frequency mode is observed at 74 cm^{-1} in infrared absorption, corresponding to the $\bar{\alpha}$ mode. Infrared measurements on the more covalent and more massive substances CuBr and CuI do not show a double peak. Thus, the $\bar{\alpha}$, $\bar{\beta}$, and $\bar{\gamma}$ peaks in CuCl are infrared- and Raman-active excitations. Although an analysis[14] of the infrared reflection data[5] indicates a weak LO mode between $\bar{\beta}$ and $\bar{\gamma}$, only one LO mode is observed in Raman scattering. The intermediate LO is probably too weak to be observed in the presence of $\bar{\beta}$ and $\bar{\gamma}$. The Raman and infrared strengths of $\bar{\gamma}$ are complementary at

TABLE I. Raman-scattering parameters.

T (°K)	ν (cm^{-1})					2Γ (cm^{-1})				$S/L\,d\Omega$ (10^{-7} cm^{-1} sr^{-1})					$(\bar{n}+1)$				
	$\bar{\alpha}$	$\bar{\beta}$	$\overline{\beta\gamma}$	$\bar{\gamma}$	$\bar{\delta}$	$\bar{\alpha}$	$\bar{\beta}$	$\bar{\gamma}$	$\bar{\delta}$	$\bar{\alpha}$	$\bar{\beta}$	$\overline{\beta\gamma}$	$\bar{\gamma}$	$\bar{\delta}$	$\bar{\alpha}$	$\bar{\beta}$	$\overline{\beta\gamma}$	$\bar{\gamma}$	$\bar{\delta}$
105	76	143	157	172	211	7.5	15	19	12	0.09	1.57	3.47	1.90	3.57	1.55	1.16	1.11	1.13	1.06
138	70	136	151	167	207	17	20	18	21	0.40	1.47	2.94	1.47	3.36	1.93	1.32	1.26	1.21	1.13
190	69	130	147	166	206	22	28	24	24	1.11	1.90	3.36	1.46	2.66	2.46	1.70	1.49	1.40	1.27
239	68	127	145	166	204	28	32	24	36	2.49	2.67	4.03	1.36	3.31	2.98	1.87	1.72	1.58	1.41
295	68	123	141	162	196	26	35	23	47	2.80	2.81	3.76	0.95	3.10	3.54	2.22	2.01	1.83	1.62

300 °K, suggesting that the lattice somehow appears centrosymmetric for this mode at elevated temperature.

The double peak seems to be intrinsic to cubic CuCl and is probably due to lattice anharmonicity. However, the peaks cannot be separately assigned to a fundamental and a two-phonon process in a satisfactory way because of the curious temperature dependence of the $\bar{\gamma}$-mode strength. Nevertheless, recent neutron scattering work,[15] which does not show a double peak, suggests that $\bar{\gamma}$ and $\bar{\delta}$ are the TO and LO modes, respectively, and that $\bar{\alpha}$ and $\bar{\beta}$ are combinations of zone-boundary phonons, in agreement with the infrared[5] and earlier Raman[6] assignments.

One way to handle the double peak is to introduce the notion of a strongly frequency-dependent damping factor[16,17] for the TO mode. Barker[18] finds that the TO mode in GaP, observed in Raman or infrared experiments, is asymmetrical while the LO is symmetrical. The frequency of $TA(X)+LA(X)$ is close to but smaller than $TO(\Gamma)$. He accounts for the observed line shape by assuming a Lorentzian TO mode with frequency-dependent damping proportional to the joint density of states in LA + TA, which should peak near the zone boundary. The damping at the higher $LO(\Gamma)$ frequency is assumed to be insensitive to frequency since it is far from the peak in damping factor. A similar mechanism can be invoked to account qualitatively for the CuCl spectrum. We assume the near coincidence with the $TO(\Gamma)$ mode of a peak in the joint density of states for the sum (or difference) of two branch frequencies at symmetrical points in the Brillouin zone. The frequency interval between the density peak and the fundamental TO frequency must be greater than the density width to give two spearate peaks. Such a narrow band of density would occur if the slopes of the two participating bands, say, LA + TA near the zone boundary, were opposite. With the foregoing interpretation one simply regards the total strength of $\bar{\beta}\bar{\gamma}$ bands as the fundamental TO without giving either peak special status. The temperature dependence of the area under the $\bar{\beta}\bar{\gamma}$ peaks should then be proportional to the one-phonon Bose factor $(\bar{n}+1)$ integrated over the double peak[17] or, approximately, to $(\bar{n}+1)$ taken at the geometric mean of $\bar{\beta}$ and $\bar{\gamma}$ frequencies $\bar{\omega}$. The measurements, in fact, are in fair agreement with this prediction.

Alternatively, one would have to select $\bar{\beta}$ or $\bar{\gamma}$ as the fundamental TO and the other as a two-phonon mode. In contrast to previous work,[4-6,15] our results indicate that $\bar{\beta}$ acts more nearly like a TO.

III. ELECTRO-OPTIC AND DIELECTRIC MEASUREMENTS

A. Electro-Optic Experiments and Results

1. *Crystals*

Both crystals used were among the melt-grown samples furnished by Sharp Corp. One of the crystals was grown with no flux and had (111), $(1\bar{1}0)$, and $(1\bar{1}2)$ faces. Measurements were made with the modulating electric field in the [111] direction and with either [111] or $[1\bar{1}2]$ polarizations and with propagation in the $[1\bar{1}0]$ direction. This crystal showed some spurious birefringence but it was possible to find regions where the polarizations used were not affected. The second crystal, grown with flux, was furnished with (001), (110), and $(1\bar{1}0)$ faces. The modulating field used was parallel to the [110] direction with propagation in the $[1\bar{1}0]$ direction and polarization in the $(1\bar{1}0)$ plane and at $\pm 45°$ to [001]. This sample, which was used for the temperature runs, was not birefringent.

2. *Experiment*

Electro-optic measurements were made at 0.633 and at 3.39 μm using the heterodyne method. Modulating frequencies of from 50 to 90 MHz were used in the course of the experiments and since there was no evidence of acoustic resonances the electro-optic values found are for constant strain. Platinum paste electrodes provided contact to the crystals. Field strengths as high as 1500 V/cm were applied when the crystal was mounted on a copper block and in air, although the measurements were made at lower fields because of heating of the crystal. Heating is evidenced either by dielectric-constant changes which cause detuning of the resonant circuit of which the crystal is part or, more sensitively, by beam deflection or deterioration due to nonuniform strains. The latter is particularly evident at 0.633 μm. When the crystal was mounted on a copper block in vacuum, field strengths as low as 500 V/cm caused appreciable beam distortion. In order to avoid heating, many of the measurements were made by applying the modulating field for times of about 1 sec with relatively long times between measurements. Results obtained in this fashion were in reasonable agreement with those found using steady but smaller fields and consequently a poorer signal-to-noise ratio.

In the course of making the 0.633-μm measurements, a continuous deterioration of the beam transmitted through the crystal was noted. This occurred when the ~50-μW beam was focused in the crystal, producing an intensity of about 20 W/cm^2. This power density damaged the crystal in what is apparently an irreversible fashion, the damage resulting in distortion of the laser beam. The problem was avoided by moving the crystal out of the focal point. However, the susceptibility to damage may limit the usefulness of the material in practical devices.

The temperature dependence of the electro-optic effect was found with the crystal mounted on a copper block and cooled by a Joule-Thomson refrig-

erator similar to the one used in the Raman experiments. The temperature of the block, which was varied from room temperature to 90 °K, was monitored with an accurately calibrated platinum resistance thermometer. Because of radiation losses, conduction losses associated with the radio-frequencies (rf) lead in, and the presence of rf heating, the temperature of the sample is probably not known to an accuracy better than 5 °K.

3. *Results*

The room-temperature values of the constant-strain electro-optic coefficient r_{41} were -2.35×10^{-12} m/V at 0.633 μm and -2.5×10^{-12} m/V at 3.39 μm. Our earlier measurements[19] gave the same value at 0.633 μm and 2.2×10^{-12} m/V at 3.39 μm. Because of the measurement difficulties mentioned above, the uncertainty is ± 20%. The negative sign of the coefficient is based on a recent determination[20] which uses the convention that a vector pointing from a Cu ion to a nearest-neighbor Cl ion defines a positive ⟨111⟩ direction. Recent measurements[21] of the low-frequency or constant-stress coefficient at 0.633 and 10.6 μm indicate that this coefficient also has little wavelength dependence.

As the temperature was lowered from room temperature to 90 °K the electro-optic coefficient decreased markedly: A reduction by a factor of 3 was found at 0.633 μm and a factor of 2 at 3.39 μm. Most of the measurements were made with the temperature increasing, but enough points were taken during cooling cycles to establish that there was no discernible temperature lag. The dependence of r_{41} on T was linear, as shown in Fig. 3, although there was some evidence—particularly in the 0.633-μm runs—that the slope of r_{41} vs T was smaller at the lower temperatures.

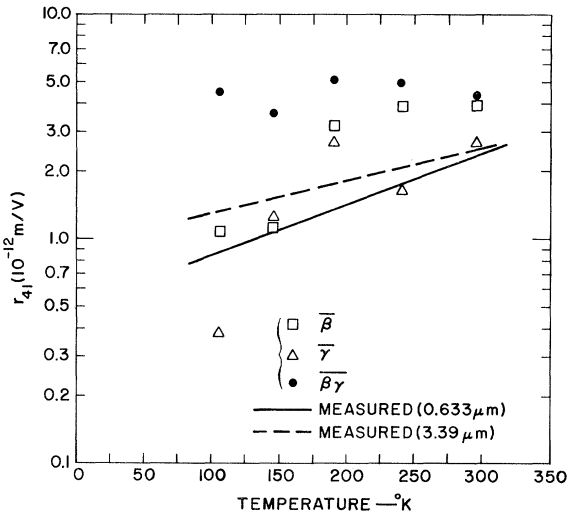

FIG. 3. Measured and calculated electro-optic coefficient r_{41} vs temperature. Curve from rf measurements. Points from Table II for $(\omega_{LO}, \omega_{TO}) = (\omega_\beta, \omega_6)$, $(\omega_\gamma, \omega_6)$, and $(\bar{\omega}, \omega_6)$.

B. Dielectric Measurements

Room-temperature measurements of the capacitance of two samples were made in the frequency range 5–110 MHz. The value found did not vary with frequency and the calculated constant-strain relative dielectric constant κ was found to be 7. The accuracy of this determination was limited by irregularities in sample shape, the small capacitances involved (1.0 and 1.83 pF for the two crystals), and by the necessity for fringing field corrections. Thus, we have chosen to use the value $\kappa = 7.9$, which was found[22] by an infrared reflectivity measurement at 320 μm, and have used the capacitance results only in determining the percentage change due to temperature.

The temperature dependence of capacitance was measured in the same apparatus used for the electro-optic experiments. Distributed capacity, capacity of the ceramic leadthrough, and capacity of the crystal were all about equal. The self-inductance of the leads further complicated the circuit and in order to stay well away from circuit resonances the most reliable measurements were made at 7 and 14 MHz. These frequencies had previously been shown to be high enough to avoid acoustic resonances in the room-temperature work. The capacitance decreased by 0.27 pF as the temperature was lowered from 295 to 90 °K and all of this change was ascribed to reduction of the CuCl dielectric constant. Since this crystal had a room-temperature capacitance of 1.83 pF, the change was 15%. The results are shown on Fig. 4. The decrease in dielectric constant with temperature found here is in good agreement with earlier work[23] at 10 MHz.

C. Discussion

In order to correlate the temperature dependence of the electro-optic coefficient and dielectric constant, we make use of the fact that the electro-optic coefficient arises from two sources: first, a purely electronic nonlinear polarizability related to the optical-mixing coefficient d_{14}^0 and second, a term caused by the change in optical polarizability due to ionic motion (see Sec. IV). Since this same ionic motion contributes to the dielectric constant κ, a change in κ results in a proportional change in the ionic term in r_{41}. This viewpoint is well justified in discussing the electro-optic behavior of crystals such as GaP[24] and GaAs[7] which have the same structure as CuCl.

Separating the lattice (d_{14}^i) and electronic (d_{14}^0) contributions to r_{41} we write[25]

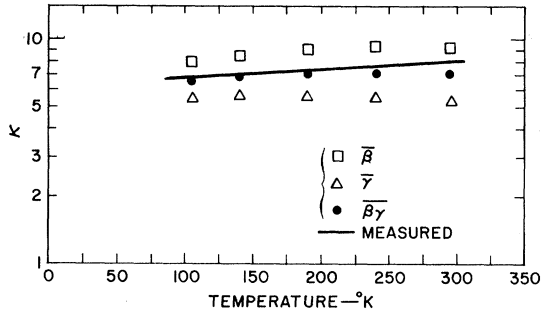

FIG. 4. Measured and calculated low-frequency dielectric constant $\kappa(0)$ vs temperature. Curve from rf and infrared measurement. Points from LST with $(\omega_{LO}, \omega_{TO}) = (\omega_\beta, \omega_\delta)$, $(\omega_\gamma, \omega_\delta)$, and $(\bar{\omega}, \omega_\delta)$.

$$n^4 r_{41} = -4d_{14}^{e0} = -4(d_{14}^i + d_{14}^0) = -4(1+C)\,d_{14}^0\,, \qquad (3)$$

where n is the refractive index and the quantity C is the lattice/electron ratio.[24] The dependence on linear susceptibilities can be shown explicitly by rewriting (3) as

$$n^4 r_{41}(T) = -4(n^2-1)^2\{[\kappa(T)-n^2]\,\delta_{14}^C + (n^2-1)\delta_{14}^D\}\,, \qquad (4)$$

where we have introduced the generalized Miller δ's $d_{14}^i \equiv (\kappa - n^2)(n^2-1)^2\,\delta_{14}^C$ and $d_{14}^0 = (n^2-1)^3\,\delta_{14}^D$. The lattice term δ^C and the electronic term δ^D are more nearly constant[26,27] in materials with similar structure than the corresponding nonlinear susceptibilities d^i and d^0. For this reason, we assume the δ's to be temperature independent. The optical frequencies used here are sufficiently far from the band edge that the refractive indices do not change[28] with temperature. However, as indicated in (4), r_{41} and κ vary with temperature.

Using the experimentally found values of $\kappa(T)$ and $r_{41}(T)$ at 90 and 295 °K, we define the ratios of ionic susceptibility,

$$\rho \equiv [\kappa(90\ ^\circ\mathrm{K}) - n^2]/[\kappa(295\ ^\circ\mathrm{K}) - n^2], \qquad (5)$$

and electro-optic coefficient,

$$R \equiv r_{41}(90\ ^\circ\mathrm{K})/r_{41}(295\ ^\circ\mathrm{K}). \qquad (6)$$

From (3) and (4) evaluated at 90 and 295 °K we find, in terms of the experimental ratios R and ρ,

$$C(295\ ^\circ\mathrm{K}) = \frac{1-R}{R-\rho} = \frac{1}{\rho}C(90\ ^\circ\mathrm{K})\,, \qquad (7)$$

$$\delta_{14}^D = -\frac{n^4}{4(n^2-1)^3}\,\frac{R-\rho}{1-\rho}\,r_{41}(295\ ^\circ\mathrm{K})\,, \qquad (8)$$

$$\delta_{14}^C = -\frac{n^4}{4[\kappa(295\ ^\circ\mathrm{K})-n^2](n^2-1)^2}\,\frac{1-R}{1-\rho}\,r_{41}(295\ ^\circ\mathrm{K}). \qquad (9)$$

In Table II we show values of C at 295 °K computed from (7) as well as values found from (3) using our values of r_{41} and published[29] values of d_{41}^0. The nonlinear coefficients δ_{14}^D and δ_{14}^C calculated from (8) and (9) using our electro-optic and dielectric results and the corresponding d_{14}^0 and d_{14}^i are also shown in Table II. For comparison, the directly measured nonlinear coefficients δ_{14}^D and d_{14}^0 are also included. The calculated results are in rather remarkable agreement with the directly measured values: Values found from our 0.633-μm measurements agree with 1.06-μm harmonic generation experiments and, similarly, our 3.39- and the 10.6-μm second harmonic generation (SHG) values agree. Although appreciable dispersion of d_{14}^0 is not expected in this spectral range, it is interesting that both the direct and indirect determinations indicate it exists.

Although the excellent quantitative agreement indicates the method used is probably correct, we should point out such good agreement is fortuitous. First, we have already indicated that the magnitude of r_{41} is uncertain to about 20%. This uncertainty carries over directly to the deduced optical coefficients. Second, the ratio R, which was 0.5 at 3.39 μm and 0.33 at 0.633 μm is also probably not known to better than 20%. This 20% uncertainty leads to a similar or larger uncertainty in the optical nonlinear coefficients. Finally, we note that both the value of the dielectric constant chosen at room temperature and the change in going to 90 °K are uncertain. For example, if the dielectric constant is reduced only 14% rather than 15% in cooling, the ratio ρ becomes 0.70 rather than 0.72 and this, in turn, leads to a 10% change in d_{14}^0.

TABLE II. Nonlinear coefficients of CuCl calculated from electro-optic and dielectric properties.

λ (μm)	d_{14}^0 (10^{-12} m/V)	δ_{14}^D (10^{-12} m/V)	d_{14}^{e0} (10^{-12} m/V)	d_{14}^i (10^{-12} m/V)	δ_{14}^C (10^{-12} m/V)	C (295 °K)
0.6328	−12	−0.53	+8.635	+20.5	+0.63	−1.7
3.39	−6.5	−0.35	+8.32	+15	+0.5	−2.3
1.06	−12.6[a]	−0.61[a]				−1.7[b]
10.6	−6.7[a]	−0.42[a]				−2.2[b]

[a]Magnitudes from D. Chemla, F. Kupecek, C. Schwartz, C. Schwab, and A. Goltzene, IEEE J. Quantum Electron. QE-7, 126 (1971). Signs from R. C. Miller, S. C. Abrahams, R. L. Barns, J. L. Bernstein, W. A. Nordland, and E. H. Turner, Solid State Commun. (to be published).

[b]Using directly measured electro-optic coefficient at 0.633 μm with the 1.06-μm d^0 and 3.39-μm d^{e0} with the 10.6-μm d^0.

IV. RELATIONSHIP BETWEEN RAMAN AND ELECTRO-OPTIC MEASUREMENTS

A. Theoretical Background

1. *Fundamental-Mode Treatment*

The electro-optic coefficient r_{41}, SHG coefficient d_{14}^0, and the ratio C of lattice and electronic contributions to r_{41} can be calculated to good accuracy from absolute Raman-scattering efficiencies for an ideal zinc-blende crystal like GaAs.[7] The treatment ignores two-phonon effects, a valid approximation in GaAs. However, two-phonon modes cannot be ignored in CuCl, where their Raman and infrared strengths match those of the fundamental modes.

The treatment for fundamental lattice modes given elsewhere[7,30] can be summarized as follows. In a principal-axis coordinate system where the optical dielectric tensor $n_{ij}^2 = n_i^2\delta_{ij}$, the Pockels electro-optic effect is defined by

$$\Delta(n^{-2})_{ij} = \sum_k r_{ij,k} E_k(\omega) = \Delta n_{ij}^2 / n_i^2 n_j^2 , \tag{10}$$

where $E_k(\omega)$ is the modulating field at angular frequency ω. The lattice and electronic contributions to the electro-optic coefficient $r_{ij,k}$ may be displayed explicitly as

$$-\epsilon_0 n_i^2 r_{ij,k} n_j^2 = \alpha_{ij,k}^m \beta_k^m(\omega) + \xi_{ijk} , \tag{11}$$

with m an optic mode index, ϵ_0 the vacuum permittivity, and

$$\alpha_{ij,k}^m = \frac{\epsilon_0 \partial \kappa_{ij}}{\partial Q_k^m} , \tag{12}$$

$$\beta_k^m(\omega) = \frac{\partial Q_k^m}{\partial E_k(\omega)} = \beta_k^m(0)\frac{\omega_m^2}{\omega_m^2 - \omega^2} , \tag{13}$$

$$\xi_{ijk} = \frac{\epsilon_0 \partial \kappa_{ij}}{\partial E_k} . \tag{14}$$

Only an acentric crystal may have a mode for which both $\alpha_{ij,k}$ and β_k are nonvanishing. The parameter $\beta_k^m(\omega)$ is independent of ω at frequencies well below the TO phonon frequency ω_m and may be evaluated at $\omega \approx 0$ for the Pockels effect. The other parameters in (11) are independent of optical wavelength far from band edges. The first term in (11) is the "lattice" contribution and the second the "nonlattice" or "pure electronic" contribution to the electro-optic effect. As we show later, (11) is a generalization of (3).

The Raman-scattering efficiency $S_{ij,k}$ for an infrared-active mode involves these same parameters. Scattering is produced by fluctuations in κ_{ij} induced by thermally excited displacements Q_k^m at TO- or LO- mode frequencies; and $S_{ij,k}$ is proportional to the squared total derivative $|d\kappa_{ij}/dQ_k^m|^2$ for the mode in question. The treatment is simplified for crystals like GaAs in which only one mode Q_k contributes to a particular κ_{ij} component, for then (a) the symmetry coordinates Q_k are the same for LO and TO displacements, and (b) summation over m in (13) is not required. Then the Stokes-scattering efficiencies for LO and TO modes are

$$S_{ij,k}^{\mathrm{LO}} = D_{\mathrm{LO}} \left| \alpha_{ij,k} + \xi_{ijk}/\beta_k(\omega_{\mathrm{LO}}) \right|^2 , \tag{15}$$

$$S_{ij,k}^{\mathrm{TO}} = D_{\mathrm{TO}} \left| \alpha_{ij,k} \right|^2 , \tag{16}$$

$$D_{\mathrm{LO,TO}} = \frac{v}{\bar{m}} \sigma_{\mathrm{LO,TO}} = \frac{v\hbar\omega_S^4(\bar{n}_{\mathrm{LO,TO}}+1)L\, d\Omega}{32\pi^2\epsilon_0^2 c^4 \bar{m}\omega_{\mathrm{LO,TO}}} , \tag{17}$$

where ω_S is the Stokes frequency and v the primitive cell volume. The second term in (15) accounts for the effect of the macroscopic field E_k associated with the LO displacement. Since the partial change in κ_{ij} produced directly by Q_k is given by the first term, the second term includes only the *partial* change produced by E_k with Q_k clamped, i.e., only the nonlattice contribution.

Optic lattice modes are clamped when the modulating frequency ω is well above ω_{TO}, e.g., at optical frequencies, because then $\beta_k(\omega)$ vanishes. With optic modes clamped only the second term contributes to $r_{ij,k}$ in (11) and the physical process, although *an* electro-optic effect, is more specifically optical mixing or, when the frequencies of the incident and modulating fields are identical, SHG. Thus, ξ_{ijk} can be identified with an optical-mixing coefficient,[25] or, with the SHG coefficient d_{kji} (SHG) when dispersion near band edges can be neglected,

$$\xi_{ijk} = 4\epsilon_0 d_{kji}(\mathrm{SHG}) . \tag{18}$$

For zinc-blende crystals, only the nonvanishing second-rank tensor element has indices $(ijk) = 123$ or permutations thereof. Then (11) becomes[7]

$$-\epsilon_0 n^4 r_{12,3} = \alpha_{12,3}\beta_3(0) + \xi_{123} \equiv \alpha_{12,3}\beta_3(0)(1 + C^{-1}), \tag{19}$$

where C is again the lattice/electron ratio used earlier:

$$C = \alpha_{123}\beta(0)/\xi_{123} = d_{41}^i/d_{41}^0 . \tag{20}$$

The identity of (19) and (3) is apparent when we substitute the reduced coefficients: $r_{12,3} \equiv r_{41}$, $\xi_{123} \equiv 4\epsilon_0 d_{14}^0$, and $\alpha_{12,3}\beta_3(0) \equiv 4\epsilon_0 d_{14}^i$. The quantity $\beta_3(0)$ can be written in terms of spring constant K or effective ionic charge Z,

$$\beta_3(0) = (\epsilon_0 \Delta\kappa v/K)^{1/2} = \epsilon_0 \Delta\kappa v/Z = Z/K, \tag{21}$$

with $\Delta\kappa = \kappa - n^2$, the lattice susceptibility or infrared strength of the lattice mode. The latter form illustrates the explicit dependence of d_{14}^i on $\Delta\kappa$ indicated in (4).

The nonlinear coefficients can be obtained from Raman measurements by means of the following formulas[7] obtained from (15)–(20):

$$C^{-1} = a[1 \pm (\sigma_{TO} S_{LO}/\sigma_{LO} S_{TO})^{1/2}], \quad (22)$$

$$r_{41}^2 = S_{TO} n_\infty^2 (1 + C^{-1})^2/\epsilon_0 n^8 a \omega_{TO}^2 \sigma_{TO}, \quad (23)$$

$$d_{14}^0 = -n^4 r_{41}/4(1 + C), \quad (24)$$

where

$$a = \omega_{TO}^2(\omega_{LO}^2 - \omega_{TO}^2)^{-1}, \quad (25)$$

$\sigma_{LO,TO}$ is given by (17), n is the refractive index at the optical frequency, and n_∞ is the "high-frequency" (dispersionless) refractive index. The square root leads to an ambiguity in the calculation of C in (22). As a rule the values of r_{41} or d_{14}^0 calculated from (23) or (24) with the two choices of C differ sufficiently that the correct choice of C can be made by comparison with crude direct measurements of r_{41} or d_{14}^0. The absolute signs of r_{41} and d_{14}^0 cannot be determined by Raman measurements, but their relative sign is given by (3) or (24).

The treatment is more complicated for multimode crystals, such as $LiTaO_3$, that have more than two atoms per unit cell. In this case, if infrared strength $\Delta\kappa_k^m$, which is the contribution of the m mode to the low-frequency dielectric constant κ_k, is known for each mode, then[30]

$$-\epsilon_0 n_i^2 n_j^2 r_{ij,k} = \sum_m \pm \left(\frac{\epsilon_0 \Delta\kappa_k^m S_{ij,k}^m}{\sigma_{TO}^m}\right)^{1/2} + \xi_{ijk}, \quad (26)$$

where $S_{ij,k}^m$ and σ_{TO}^m refer to the appropriate TO mode and the sign ambiguity for each term of the summation arises from the square root.

2. *Two-Phonon Modes*

The preceding treatment can be adapted to take account of two-phonon effects in a straightforward way by introducing generalized symmetry coordinates Q_k^m for each mode, whether of one or two phonon origin. In this case, (26) would be applied to the CuCl results with $m = \bar{\alpha}$, $\bar{\beta}$, $\bar{\gamma}$ or $m = \bar{\alpha}$, $\overline{\beta\gamma}$, if $\overline{\beta\gamma}$ is regarded as a combined mode. Since the corresponding $\Delta\kappa_k^m$ have not been measured, it is not possible to make quantitative comparisons without further approximation. For example, if one mode accounts for most of the dielectric constant, so that all other $\Delta\kappa_k^m$ are negligible and only one term remains in the summation, then the single-mode formulation would apply directly. We will find that either $\bar{\beta}$ or $\overline{\beta\gamma}$ is a reasonable choice for the effective mode.

B. Lyddane-Sachs-Teller Comparison

A calculation[14] based on published infrared-absorption measurements[5] indicates that the $\bar{\alpha}$ mode contributes less than 15% to κ at 20 °K. An examination of the generalized Lyddane-Sachs-Teller (LST) relations also gives an indication of relative contributions of the various modes. If $\bar{\beta}$ and $\bar{\delta}$ are taken as TO and LO and $\bar{\alpha}$ and $\bar{\gamma}$ are ignored, the LST relation for the low-frequency dielectric constant κ is

$$\kappa = (\omega_\delta/\omega_\beta)^2 n_\infty^2; \quad (27)$$

and a similar equation holds if $\bar{\gamma}$ and $\bar{\delta}$ are taken as TO and LO. The results of such calculations with[12] $n_\infty^2 = 3.61$ are plotted in Fig. 4. The $\bar{\gamma} - \bar{\delta}$ combination gives a temperature-independent constant, as shown by Krauzman,[6] but the measured κ in fact increases with T.

If $\bar{\beta}$ and $\bar{\gamma}$ modes both have appreciable infrared strengths, they should be separated by a LO mode.[1] Since this intermediate mode is not observed, we take its frequency to be the geometric mean of the $\bar{\beta}$ and $\bar{\gamma}$ frequencies, i.e., $\bar{\omega} = (\omega_\beta \omega_\gamma)^{1/2}$. Then the generalized LST relation for the two modes is

$$\kappa = (\bar{\omega}/\omega_\beta)^2(\omega_\delta/\omega_\gamma)^2 n_\infty^2 = (\omega_\delta/\bar{\omega})^2 n_\infty^2, \quad (28)$$

which is the same result one would obtain by taking the geometric mean of the double-peaked $\overline{\beta\gamma}$ mode as the TO and $\bar{\delta}$ as the LO. This result is also plotted in Fig. 4. The directly measured dielectric constant of Sec. III is also shown. It can be seen that the $\overline{\beta\gamma}$ mode gives the best agreement; the β mode gives a κ that is somewhat large; and the γ mode gives a κ that is much too small.

C. Calculation of Nonlinear Coefficients

We can now apply the single-mode formulas (22)–(24) to find C, r_{41}, and d_{14} for the three cases: (i) $\omega_{TO} = \omega_\beta$, $\omega_{LO} = \omega_\delta$; (ii) $\omega_{TO} = \omega_\gamma$, $\omega_{LO} = \omega_\delta$; (iii) $\omega_{TO} = \bar{\omega} = (\omega_\beta \omega_\gamma)^{1/2}$, $\omega_{LO} = \omega_\delta$; and we can compare the results with direct measurements. The calculated values are given in Table III for both the upper (+) and lower (−) sign in (22). The absolute signs of r_{41} and d_{14}^0 cannot be determined by the analysis. However, based on Ref. 20, the sign of r_{41} is taken negative and the tabulated signs of d_{14}^0 follow from (24). Comparison of $r_{41}^{\pm}$ with the measured r_{41} (Sec. III) clearly indicates that r_{41}^- is the correct choice, allowing for a factor-of-2 uncertainty in measured S_{LO} and S_{TO}. The choice of the lower (−) sign in (22) is consistent with the directly measured[20] negative signs of r_{41} and d_{14}^0, since the fact that they have the same sign requires $C < -1$. The calculated and measured r_{41} are plotted in Fig. 3. The corresponding values of C^- are negative and in the order of unity. Examination of (23) and (24) shows that errors in C give give rise to large errors in r_{41} and d_{14} when $C \approx -1$.

D. Discussion

The correlation between measured and calculated r_{41} presented in Fig. 3 is best for case (i), ω_{TO}

TABLE III. Nonlinear coefficients calculated from single-mode formulas taking ω_β, ω_γ, or $\bar{\omega}$ as the TO frequency and ω_δ as the LO frequency.

	C^+			r_{41}^+ (10^{-12} m/V)		
T (°K)	$\bar{\beta}$	$\bar{\gamma}$	$\overline{\beta\gamma}$	$\bar{\beta}$	$\bar{\gamma}$	$\overline{\beta\gamma}$
105	0.400	0.197	0.365	(−)18.3	(−)21.5	(−)23.4
138	0.434	0.195	0.380	(−)17.0	(−)19.0	(−)21.1
190	0.562	0.209	0.449	(−)16.2	(−)16.8	(−)19.5
239	0.599	0.180	0.444	(−)17.6	(−)16.8	(−)20.3
295	0.600	0.149	0.422	(−)9.67	(−)14.8	(−)18.5

	C^-			r_{41}^- (10^{-12} m/V)			d_{14}^- (10^{-12} m/V)		
T (°K)	$\bar{\beta}$	$\bar{\gamma}$	$\overline{\beta\gamma}$	$\bar{\beta}$	$\bar{\gamma}$	$\overline{\beta\gamma}$	$\bar{\beta}$	$\bar{\gamma}$	$\overline{\beta\gamma}$
105	−1.26	−0.90	−3.60	(−)1.07	(−)0.38	(−)4.53	(−)15.4	(+)20.1	(−)8.15
138	−1.27	−0.71	−2.66	(−)1.11	(−)1.25	(−)3.63	(−)15.0	(+)16.1	(−)8.10
190	−2.19	−0.92	−6.40	(−)3.27	(−)2.59	(−)5.10	(−)9.85	(+)116.9	(−)3.50
239	−2.47	−0.61	−5.07	(−)3.93	(−)1.65	(−)5.00	(−)9.89	(+)15.6	(−)4.55
295	−2.73	−0.41	−4.68	(−)3.95	(−)2.70	(−)4.33	(−)8.45	(+)17.1	(−)4.36

$=\omega_\beta$. The agreement for r_{41} at room temperature is satisfactory for all three cases. In view of the experimental and computational difficulties involved, agreement within a factor of 2 is considered quite good. The temperature dependence agrees within experimental uncertainty for both the $\bar{\beta}$ and $\bar{\gamma}$ results, but the $\overline{\beta\gamma}$ result does not show any temperature dependence and is in substantial disagreement at 105 °K.

The SHG coefficient d_{14}^0 has been directly measured[29] as 6.7×10^{-12} m/V at 10.6 μ and 12.6×10^{-12} m/V at 1.06 μ and is negative[20] in sign. The average measured d_{14}^0 at 295 °K is then -9.7×10^{-12} m/V, in good agreement with the $\bar{\beta}$ and in fair agreement with $\overline{\beta\gamma}$ values in Table III. The C values calculated from the single-mode formula (24) using the 10.6- and 1.06-μ values of d_{14}^0 and measured r_{41} are −2.2 and −1.7, respectively. These values fit within experimental uncertainty the C^- calculated for the $\bar{\beta}$ mode listed in Table III.

Thus, we find that a single-mode calculation taking $\bar{\beta}$ to be the TO and $\bar{\delta}$ the LO mode, neglecting the other modes, gives a reasonably good representation of the directly measured r_{41}, d_{14}, and C. Still a proper comparison would require direct infrared measurements of the strengths of $\bar{\alpha}$, $\bar{\beta}$, and $\bar{\delta}$ modes in order to determine $\Delta\kappa_k^m$ for use in (26). Moreover, the calculation of nonlinear coefficients from spectra involving strong two-phonon effects needs to be put on a firmer theoretical base than we have done.

V. COMPARISON OF PROPERTIES OF CuCl AND GaAs

Zinc blende is the simplest structure that lacks a center of inversion and therefore exhibits both a linear electro-optic effect and a second-order nonlinear susceptibility. A single optic mode that is both Raman and infrared active is responsible for the electro-optic effect. The range of properties among the large number of binary crystals with this structure is attributed to the nature of the bonding in each compound,[1,2] i.e., the relative importance of covalent and ionic forces. Since CuCl is largely ionic while GaAs is largely covalent, it is interesting to make quantitative comparisons between the measured and derived properties of the two crystals. If one constructs a simple bond-oscillator model[16] based on established notions of covalency and ionicity, then it is possible to account for some of the differences in properties in a qualitative fashion. The model attempts to account for the properties of a crystal based on the properties of an isolated bond; the model neglects local fields and interactions with neighboring bonds. These shortcomings become evident when the model is applied to microscopic rather than macroscopic properties.

A. Bond Oscillator Model

The picture presented here is largely a composite of those given by several authors, including Levine,[31,32] Kleinman,[33] and Flytzanis.[34,35]

Four bonds join at each metal M and nonmetal N ion, so that there are four tetrahedral bonds per MN molecule. The bond length is $\frac{1}{4}\sqrt{3}a$ with a the lattice constant. It is assumed that the dielectric properties of the crystal can be represented by a suitable geometric sum over the contributions of individual bonds. Thus, we may get an idea of the behavior of the tetrahedral bond by considering a single effective linear bond.

The effective bond terminated by nuclear core charges Z_M and Z_N for the metal and nonmetal atoms, respectively, is shown in Fig. 5. For most zinc-blende–type substances, Z_M and Z_N are obtained by stripping away the outer s and p electrons.

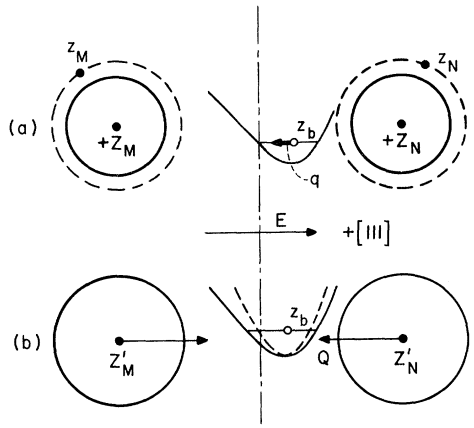

FIG. 5. Linear-bond model for GaAs. (a) Valence bond charge z_b in potential U_s (symmetric) + U_{as} (antisymmetric) with charge displacement q for positive E. (b) Covalent-bond charge z_b and ionic charges Z_M' and Z_N' with lattice displacement Q for positive E.

Thus, for GaAs, $Z_M = +3$ and $Z_N = +5$. However, in copper the ten outer d electrons are bound to the core with about the same energy as the s electron and should not necessarily be considered part of the core. Thus, for CuCl, $Z_M = +1$ or $+11$ and $Z_N = +7$. Levine[32] is able to account for the experimentally observed magnitude and sign of d_{14}^0 by the choice $Z_M = +11$. Hence, in CuCl the metal core is the more positive but in most other compounds, such as GaAs, the nonmetal core is more positive.

The valence charge of eight electrons in GaAs and 18 in CuCl is distributed throughout the cell. However, for purposes of discussion, the valence charge can be separated into atomic charges z_m and z_n localized on the metal and the nonmetal, and a bond charge z_b. The pseudopotential calculations of Walter and Cohen[36] show that the atomic charges are small in a covalent substance like Ge and z_b is centered on the bond. In GaAs, on the other hand, they find a smaller z_b displaced toward the more positive nonmetal core (As) as well as charges z_M and z_N with $z_N > z_M$. By analogy, in CuCl we expect that z_b will be displaced toward the more positive metal core (Cu) and that $z_M > z_N$. Furthermore, Walter and Cohen[36] show that z_b is proportional to $f_c - f_i$, where $f_c = 0.785$ is the critical ionicity for the zinc-blende–to–rocksalt transition.[2] Thus, in agreement with our notion of ionicity, z_b will be small in CuCl.

The preceding discussion is consistent with the *one-dimensional* potential-energy function U for the valence charge as shown in Fig. 5. The electron displacement is q. For a purely covalent bond with identical atoms and $z_M = z_N = 4$ (as in germanium) $U = U_s$ is symmetric about the bond center. As the nuclear charge difference increases, for more ionic substances, an antisymmetric component U_{as} is introduced so as to skew the potential toward the more positive core. If now we apply a positive electric field, where the positive direction is conventionally taken from metal to nonmetal, the bond charge will move in the negative direction. For GaAs, illustrated by Fig. 5, the charge moves toward the "soft" region of the asymmetric potential and the linear electronic susceptibility $\chi_q = n_\infty^2 - 1$ increases.[33] In CuCl, on the other hand, the asymmetric potential is skewed in the opposite direction and the bond charge moves toward the "hard" region of U. Thus

$$\epsilon_0 \frac{\partial \chi_q}{\partial E} = \xi_{14} = 4\epsilon_0 d_{14}^0 > 0 \quad \text{(GaAs)}\,,$$
$$\epsilon_0 \frac{\partial \chi_q}{\partial E}\ \xi_{14} = 4\epsilon_0 d_{14}^0 < 0 \quad \text{(CuCl)}\,. \tag{29}$$

Moreover, the magnitude of the above derivative is proportional to the skew component U_{as} of the potential and to the bond charge. [A deviation from (29) which need not concern us here occurs when the atomic radii of M and N differ widely.[31]] Thus, d_{14}^0 is expected to be positive for GaAs and negative for CuCl, and the nonlinear Miller coefficient[37] $\delta_{14} = d_{14}^0/\chi_q^3$, which is suitably normalized by the linear susceptibility to take account of valence-charge density, is expected to be larger for CuCl. In the preceding discussion we have mixed macroscopically defined quantities like χ_q, d_{14}, and δ_{14} with the notion of a microscopic valence charge. In particular, we have made the assumption that the macroscopic field E acts on the valence charge.

The valence charge may be separated into a bond charge and atomic charges localized on the cores to give net macroscopic ionic charges Z_M' on M and Z_N' on N. If all the valence charge were transferred to the more positive cores, as in an ideal ionic compound, $Z_N' = -Z_M'$, and the ionic charges would be ± 3 in GaAs and ∓ 7 (or ± 1) in CuCl. For a partially ionic substance, where $z_b \neq 0$, $Z_N' \neq Z_M'$, the response of the bond dipole to electric fields at frequencies greater than acoustic resonances of the sample must leave the center of mass fixed. To describe the response we define an effective dynamic ionic charge $Z = \frac{1}{2}(Z_M' - Z_N')$. In Fig. 5, the bond length is Q and the spring constant is K. A positive field acting on $\pm Z$ reduces Q when $Z_M' > Z_N'$ and increases Q when $Z_M' < Z_N'$, the change being proportional to Z/K. Thus,

$$\frac{\partial Q}{\partial E} = \beta = <0, \quad Z_M' > Z_N'$$
$$\frac{\partial Q}{\partial E} = \beta = >0, \quad Z_M' < Z_N'\,. \tag{30}$$

From (21), with v the volume per MN molecule, i.e., the volume of the primitive cell $\frac{1}{4}a^3$, the mag-

nitude of β is seen to be large for ionic crystals because the lattice susceptibility Δ_K is large and the spring constant K small.

The spatial extent of the potential function for z_b is a function of the bond length Q. When Q is reduced the symmetric potential curve becomes steeper and the electronic susceptibility χ_a is reduced so that

$$\epsilon_0 \frac{\partial \chi_a}{\partial Q} = \alpha > 0. \tag{31}$$

The change in χ_a induced by a change in Q is due to deformation of the bond charge z_b, which is proportional to $f_c - f_i$.[36] In our one-dimensional model, we consider only changes in χ_a along the bond and, following Flytzanis,[35] neglect changes normal to the bond.

The sign of the product $\alpha\beta$, which is the lattice contribution to the electro-optic effect, depends on the sign of β in (30). Direct measurements[20,26] of r_{41} and d_{14} show that $\alpha\beta < 0$ for GaAs and $\alpha\beta > 0$ for CuCl. Since the sign of α is positive and does not depend on the asymmetry of the bond, $\beta < 0$ for GaAs and $\beta > 0$ for CuCl. Then from (30) the metallic ionic charge Z'_M is more positive in GaAs and the nonmetallic ionic charge Z'_N is more positive in CuCl; i.e., $Z > 0$ for GaAs and $Z < 0$ for CuCl.

Finally, we note that in order to obtain a large lattice contribution the bond must be both ionic for large β and covalent for large α.

B. Comparison

The properties of CuCl and GaAs are compared in Table IV. The derived quantities can often be obtained in a number of ways and the method employed is indicated in the table. If a sign is not indicated explicitly, it has not been determined.

It is seen that the magnitude of δ_{14} is four times greater in CuCl than GaAs, although d^0_{14} is bigger for GaAs because of its larger refractive index. This result implies a greater asymmetric potential U_{as} for the more ionic substance. For both crystals, $C < 0$ but $|C|$ is greater for CuCl, in-

TABLE IV. Comparison of the properties of CuCl and GaAs.

	CuCl	GaAs
f_i	0.75[a]	0.31[a]
κ	7.9[b]	13.1[c]
n_∞^2	3.61[d]	11.1[c]
r_{41} (10^{-12} m/V)	−2.2[e,f]	−1.5[g,h]
d_{13} (10^{-12} m/V)	−9.7[f,i]	+140[g,j,k]
$\delta_{14} = d_{14}(n_\infty^2 - 1)^{-3}$ (10^{-12} m/V)	−0.55	+0.14
$C = -[1 + (n_\infty^4 r_{41}/4d_{14})]$	−1.74	−0.59
$\xi/\epsilon_0 = 4d_{14}$ (10^{-12} m/V)	−39	+560
$\alpha\beta/\epsilon_0 = C\xi/\epsilon_0$ (10^{-12} m/V)	+68	−330
ν_{LO} (10^2 m^{-1})	196[e]	292[g]
ν_{TO} (10^2 m^{-1})	123[β], 141[$\overline{\beta\gamma}$], 162[γ][e]	269[g]
$\overline{m}$ (amu)	22.8	36.2
$\overline{m}$ (10^{-26} kg)	3.81	6.05
a (10^{-10} m)	5.41	5.65
$v = \frac{1}{4}a^3$ (10^{-30} m^3)	39.6	45.1
$K = (2\pi\nu_{TO})^2\overline{m}$ (N/m)	20.5[β], 26.9[$\overline{\beta\gamma}$], 35.5[γ]	155
e^*_T/e	1.24[β], 1.11[$\overline{\beta\gamma}$], 0.90[γ]	2.18
e^*_S/e	0.66[β], 0.59[$\overline{\beta\gamma}$], 0.48[γ]	0.50
$\beta = e^*_T/K$ (10^{-21} m^2/V)	9.7[β], 6.6[$\overline{\beta\gamma}$], 2.54[γ]	2.2
$S_{LO}/L\ d\Omega$ (10^{-5} m^{-1})	3.1 (at 0.633 μm)[e]	23 (at 1.06 μm)[g]
$S_{TO}/L\ d\Omega$ (10^{-5} m^{-1})	2.8[β], 3.8[$\overline{\beta\gamma}$], 0.95[γ][e]	15[g]
$\sigma_{LO}/L\ d\Omega$ (10^{-2} J sec^2/F m)	1.74	1.83
$\sigma_{TO}/L\ d\Omega$ (10^{-2} J sec^2/F m)	3.85[β], 3.02[$\overline{\beta\gamma}$], 2.39[γ]	2.05
$\alpha_{LO} = [\overline{m}S_{LO}/v\sigma_{LO}]^{1/2}$ (10^{-1} F/m^2)	1.31	4.1
$\alpha_{LO} = [\overline{m}S_{TO}/v\sigma_{LO}]^{1/2}$ (10^{-1} F/m^2)	0.84[β], 1.10[$\overline{\beta\gamma}$], 0.62[γ]	3.1
$\alpha_{TO}\beta/\epsilon_0$ (10^{-12} m/V)	92[β], 82[$\overline{\beta\gamma}$], 29[γ]	770

[a]Reference 2.
[b]Reference 22.
[c]M. Hass, in *Semiconductors and Semimetals*, edited by R. K. Willardson and A. C. Beer (Academic, New York, 1967), Vol. 3.
[d]Reference 12.
[e]This paper.
[f]Reference 20.
[g]Reference 7.
[h]Reference 26.
[i]Reference 29 (mean of 10.6- and 1.06-μ values).
[j]J. H. McFee, G. D. Boyd, and P. A. Schmidt, Appl. Phys. Letters 17, (1970).
[k]J. J. Wynne and N. Bloembergen, Phys. Rev. 188, 1211 (1969).

dicating a relatively larger lattice contribution, although because of the lattice and electronic susceptibilities the absolute value of $\alpha\beta$ is greater for GaAs.

The reduced mass $\bar{m}$ and lattice constants for the two substances are comparable but the spring constant K obtained from $\bar{m}$ and the lattice frequency $\omega_{TO} = 2\pi c \nu_{TO}$ is nearly eight times greater for GaAs, if the $\bar{\beta}$ mode is taken to be the TO mode. Thus, the TO frequency decreases as ionicity increases because Coulomb forces give a softer bond than covalent overlap forces. At $f_i = f_c$, a crystal would undergo a phase transition from fourfold (zinc-blende) to sixfold (rock-salt) coordination, reflecting the spherical symmetry of the closed-shell configuration in the pure-ionic case. The situation is reminiscent of the soft-mode behavior of ferroelectric crystals where

$$\omega_{TO}^2 \sim (T - T_c) \sim \Delta K^{-1} \tag{32}$$

near the Curie temperature T_C. Martin, Lucovsky, and Burstein[38] have noted that if ionicity determines bond forces, then

$$\omega_{TO}^2 (\epsilon_0 \bar{m} v / Z^2) \sim (f_c - f_i) \sim \Delta K^{-1} \tag{33}$$

near f_c. Thus, if f_i could be adjusted (by hydrostatic pressure, for example), then one should observe $\omega_{TO} \to 0$ as one approaches the phase transition.

The effective ionic charge corresponding to the macroscopic Z, i.e., the Born charge e_T^*, can be determined from vibrational frequencies,[39]

$$Z^2 \equiv e_T^{*2} = \epsilon_0 n_\infty^2 \bar{m} v (\omega_{LO}^2 - \omega_{TO}^2) . \tag{34}$$

One can also determine a microscopic Szigetti charge e_S^* assuming an effective depolarizing field $\frac{1}{3}P$,[39]

$$e_S^* = \frac{3 e_T^*}{n_\infty^2 + 2} . \tag{35}$$

The sign of the charge cannot be determined. Questions of local fields and screening complicate the interpretation of these quantities but we see that Z in GaAs is about twice that in CuCl for the $\bar{\beta}$ mode, even though CuCl is more ionic. However, $\beta = Z/K$ for CuCl is 4.5 times that for GaAs.

The TO Raman polarizability α can be obtained from the scattering efficiency S_{TO} by (see Sec. IV)

$$|\alpha|^2 = \frac{\bar{m} S_{TO}}{\sigma v} . \tag{36}$$

We find that α for GaAs is 37 or 28 times that for CuCl for the $\bar{\beta}$ mode or $\overline{\beta\gamma}$ mode, respectively. Flytzanis[35] has shown that

$$\alpha \sim (1 - f_i) \chi_q . \tag{37}$$

Using the values in Table IV, we find the ratio of $(1 - f_i)\chi_q$ for GaAs and CuCl to be 10.7. However, if we modify (37) to reflect the observation of Walter and Cohen[36] that the bond charge—and, hence, α—vanishes at $f_i = f_c$, we have

$$\alpha \sim (f_c - f_i) \chi_q . \tag{38}$$

Then, with the observed ratios of α and Phillips's empirical values $f_c = 0.785$, $f_i(\text{GaAs}) = 0.310$, (38) gives $f_i(\text{CuCl}) = 0.74$ and 0.72 for the $\bar{\beta}$ and $\overline{\beta\gamma}$ modes, respectively. Either of these values is satisfactorily close to the value $f_i(\text{CuCl}) = 0.75$ calculated[2] from the dielectric constant.

The product $\alpha\beta/\epsilon_0$ obtained from α and β separately at the end of Table IV is seen to compare reasonably well with $\alpha\beta/\epsilon_0$ obtained from the directly measured r_{41} and d_{14}^0.

ACKNOWLEDGMENTS

We are grateful to T. Inoguchi and A. F. Armington for providing us with samples, to A. S. Barker, Jr., for making the infrared measurements and analyses mentioned in the text and for many useful discussions, to R. H. Stolen for making an infrared measurement of κ, to S. C. Abrahams for x-ray powder-pattern measurements on our samples, and to B. F. Levine for the use of his theoretical results prior to publication.

We are also grateful to L. W. Stulz and W. N. Leibolt for their excellent technical assistance.

[1] L. Pauling, *The Nature of the Chemical Bond* (Cornell U.P., Ithaca, N. Y., 1960); Phys. Today 24, 9 (1971).

[2] J. C. Phillips, Rev. Mod. Phys. 42, 317 (1970); J. A. VanVechten, Phys. Rev. 182, 891 (1969); 187, 1007 (1969).

[3] A. Mooradian, *Advances in Solid State Physics*, Vol. 9 (Pergamon, New York, 1969).

[4] S. Iwasa and E. Burstein, J. Phys. Radium 26, 614 (1965).

[5] J. A. Plendl, A. Hadni, J. Claudel, Y. Henninger, G. Morlot, P. Strimer, and L. C. Mansur, Appl. Opt. 5, 397 (1966); A. Hadni, F. Brehat, J. Claudel, and P. Strimer, J. Chem. Phys. 49, 471 (1968).

[6] M. Krauzman, in *Light Scattering Spectra of Solids*, edited by G. B. Wright (Springer-Verlag, New York, 1969); thesis (University of Paris, 1969) (unpublished).

[7] W. D. Johnston, Jr. and I. P. Kaminow, Phys. Rev. 188, 1209 (1969).

[8] K. Nakazawa, M. Koba, I. Niwa, and T. Inoguchi, Sharp Tech. J. 6, 27 (1967).

[9] A. F. Armington and J. J. O'Connor, J. Crystal Growth 3/4, 367 (1968).

[10] J. G. Skinner and W. G. Nilsen, J. Opt. Soc. Am. 58, 113 (1968).

[11] W. D. Johnston, Jr. and I. P. Kaminow, Phys. Rev. 168, 1045 (1968); 178, 1528 (E) (1969).

[12] A. Feldman and D. Horowitz, J. Opt. Soc. Am. 59, 1406 (1969).

[13] We are grateful to S. C. Abrahams for making these measurements.

[14] Analysis of Ref. 5 reflection data at 77 °K by A. S. Barker, Jr., shows TO peaks at ~150 and 180 cm^{-1} and LO peaks at ~160 and 210 cm^{-1}. At 20 °K, the 74-cm^{-1}

mode contributes less than 15% to the low-frequency dielectric constant.

[15]C. Carabatos, B. Hennion, K. Kunc, F. Moussa, and C. Schwab, Phys. Rev. Letters 26, 770 (1971).

[16]M. Born and K. Huang, *Dynamical Theory of Crystal Lattices* (Oxford U.P., London, 1966).

[17]M. Lax, J. Phys. Chem. Solids 25, 487 (1964).

[18]A. S. Barker, Jr., Phys. Rev. 165, 917 (1968).

[19]I. P. Kaminow and E. H. Turner, in *Handbook of Lasers*, edited by R. J. Pressley (Chemical Rubber Co., Cleveland, Ohio, 1971).

[20]R. C. Miller, S. C. Abrahams, R. L. Barns, J. L. Bernstein, W. A. Nordland, and E. H. Turner, Solid State Commun. 9, 1463 (1971).

[21]T. Sueta, T. Matsushima, T. Nishimoto, and T. Makimoto, Proc. IEEE 58, 1378 (1970). This paper also summarizes some other constant-stress results.

[22]R. H. Stolen, unpublished infrared measurements ($\kappa = 7.9$ at 320 and 144 μm, $\alpha = 7$ cm^{-1} at 10.7 cm^{-1}).

[23]A. Smakula, Report No. AFCRL-67-0645, AD 663734, 1967 (unpublished).

[24]W. L. Faust and C. H. Henry, Phys. Rev. Letters 17, 1265 (1966); W. L. Faust, C. H. Henry, and R. H. Eick, Phys. Rev. 133, 781 (1968).

[25]G. D. Boyd and D. A. Kleinman, J. Appl. Phys. 39, 3597 (1968). The general definition of nonlinear coefficients is given in a useful appendix. Our usage is the same although we use rationalized mks rather than cgs units. In mks units the Fourier amplitudes of a second-harmonic polarization wave and fundamental electric field waves are related by $P_x(2\omega) = \epsilon_0 d_{14}^0 E_y(\omega) E_z(\omega)$, where ϵ_0 is the vacuum permitivity. This relation defines d_{14}^0. Conversion relations are $r(\text{cgs}) = 3 \times 10^4 r(\text{mks})$ and $d(\text{cgs}) = (3 \times 10^4/4) d(\text{mks})$.

[26]G. D. Boyd, T. J. Bridges, M. A. Pollack, and E. H. Turner, Phys. Rev. Letters 26, 387 (1971).

[27]C. G. B. Garrett, IEEE J. Quantum Electron. 4, 70 (1968).

[28]Yozo Kaifu and Teruo Komatsu, J. Phys. Soc. Japan 25, 644 (1968).

[29]D. Chemla, P. Kupecek, C. Schwartz, C. Schwab, and A. Goltzene, IEEE J. Quantum Electron. 7, 126 (1971).

[30]I. P. Kaminow and W. D. Johnston, Jr., Phys. Rev. 160, 519 (1967); 178, 1528(E) (1969); W. D. Johnston, Jr., Phys. Rev. B 1, 3494 (1970).

[31]B. F. Levine, Phys. Rev. Letters 22, 787 (1969); 25, 440 (1970).

[32]B. F. Levine (unpublished).

[33]D. A. Kleinman, Phys. Rev. B 2, 3199 (1970).

[34]C. Flytzanis, Phys. Rev. Letters 23, 1336 (1969).

[35]C. Flytzanis, Phys. Letters 34A, 99 (1971).

[36]J. P. Walter and M. L. Cohen, Phys. Rev. Letters 26, 17 (1971).

[37]R. C. Miller, Appl. Phys. Letters 5, 17 (1964).

[38]R. M. Martin, G. Lucovsky, and E. Burstein, Bull. Am. Phys. Soc. 16, 427 (1971).

[39]E. Burstein, M. H. Brodsky, and G. Lucovsky, Intern. J. Quantum Chem. 1S, 759 (1967).

PHYSICAL REVIEW B VOLUME 5, NUMBER 4 15 FEBRUARY 1972

Raman-Active Optical Phonons in the Hexagonal Phases of Solid H_2, D_2, and HD

Isaac F. Silvera* and Walter N. Hardy†
North American Rockwell Science Center, Thousand Oaks, California 91360

and

John P. McTague
Department of Chemistry,‡ University of California, Los Angeles, California 90024

(Received 23 August 1971)

Raman scattering from the transverse optic phonon in the hcp phase of single crystals of the five modifications of solid hydrogen has been observed. Frequencies have been measured to a precision of 0.05 cm^{-1} and are compared with results of recent quantum-crystal theories of lattice dynamics. Reasonable agreement with theory is found, although frequency differences between ortho and para modifications of the same isotope are much larger than predicted. Absolute measurements of the phonon scattering efficiencies are made by comparing to the intensities of the $J = 1 \rightarrow 3$ or $0 \rightarrow 2$ rotational Raman lines. The results are in good agreement with Werthamer's recent theory for light scattering in van der Waals–type crystals. A broad continuous feature observed at shifts of 40–200 cm^{-1} is tentatively identified as a two-phonon band. Predictions are made for the phonon intensities expected in solid hcp helium.

I. INTRODUCTION

In the past several years there have been increasing theoretical advances in the understanding of the dynamical properties of the so-called quantum solids (notably solid He, H_2, and their isotopes). In these solids the kinetic energy of a particle associated with a lattice site is comparable to its potential energy, even at 0 K, and as a consequence the zero-point motion is substantial. This large zero-point motion and the attendant anharmonicity render the standard methods of lattice dynamics invalid and new methods have been developed.[1] The